



HAL
open science

A general analytical model for the design of conventional heat pipes

Stéphane Lips, Frédéric Lefèvre

► **To cite this version:**

Stéphane Lips, Frédéric Lefèvre. A general analytical model for the design of conventional heat pipes. *International Journal of Heat and Mass Transfer*, 2014, 72, pp.288-298. 10.1016/j.ijheatmasstransfer.2013.12.068 . hal-01026177

HAL Id: hal-01026177

<https://hal.science/hal-01026177>

Submitted on 23 Mar 2017

HAL is a multi-disciplinary open access archive for the deposit and dissemination of scientific research documents, whether they are published or not. The documents may come from teaching and research institutions in France or abroad, or from public or private research centers.

L'archive ouverte pluridisciplinaire **HAL**, est destinée au dépôt et à la diffusion de documents scientifiques de niveau recherche, publiés ou non, émanant des établissements d'enseignement et de recherche français ou étrangers, des laboratoires publics ou privés.

A GENERAL ANALYTICAL MODEL FOR THE DESIGN OF CONVENTIONAL HEAT PIPES

Stéphane Lips^{*a,b,c}, Frédéric Lefèvre^{a,b,c}

a Université de Lyon, CNRS

b INSA-Lyon, CETHIL, UMR5008, F-69621, Villeurbanne, France

c Université Lyon 1, UMR5008, CETHIL, F-69622, France

Abstract

An analytical solution is presented for the 3D temperature field and the 2D pressure and velocity fields within a conventional heat pipe either flat or cylindrical. Several heat sources and heat sinks can be located on the heat pipe. The model is a generalisation of a previous analytical solution developed for a flat plate heat pipe fully insulated on one of its face. The equivalent thermal conductivity and the permeability are the main parameters of the capillary structure. A Fourier series expansion is used to solve the 3D heat conduction equation in the heat pipe wall. A similar approach enables to solve the 2D balance equations within the liquid and the vapour. The thermal and the hydrodynamic models are coupled together. The model can be used to determine the thermal resistance and the different limits of the heat pipe. As the model is analytically derivable, it is straightforward to use it to optimize heat pipe parameters and the locations of the heat sources and the heat sinks. An inverse formulation can be derived easily to estimate the capillary structure parameters using wall temperature measurements. In the case of the classical problem of a cylindrical heat pipe heated on one side and cooled on the other side, the simplification of the general solution enables to establish the well-known theory of heat pipe modelling, which validates the approach.

Keywords: flat plate heat pipe; cylindrical heat pipe; analytical solution; permeability; equivalent thermal conductivity

* Corresponding author. Tel.: +33 4 7243 8815; fax: +33 4 7243 8811.

E-mail address: stephane.lips@insa-lyon.fr (S. Lips)

Nomenclature

a	heat pipe length, m
a_1, a_2	heat source coordinates along the x axis, m
A_{mn}, A'_{mn}	Fourier coefficients, -
b	heat pipe width, m
b_1, b_2	heat source coordinates along the y axis, m
B	non-dimensional parameter, -
B_{mn}, B'_{mn}	Fourier coefficients, -
Bi	Biot number, -
c	wall thickness, m
C	non-dimensional parameter, -
C_{mn}, C'_{mn}	Fourier coefficients, -
d	heat pipe diameter, m
D_{mn}, D'_{mn}	Fourier coefficients, -
G	parameter, -
h	heat transfer coefficient, $Wm^{-2}K^{-1}$
h_l	altitude of the capillary structure, m
h_v	latent heat of vaporization, $J kg^{-1}$
H_p	capillary structure thickness, m
H_v	vapor space thickness, m
K	permeability, m^2
$n_{source,sink}$	number of heat sources or heat sinks in the periodic domain
$\tilde{n}_{source,sink}$	number of heat sources or heat sinks in the physical domain
P	pressure, Pa
P_t	total pressure, Pa
Q	heat transfer rate, W
r	radius of curvature of the liquid-vapor interface, m
r_{eff}	effective pore radius, m
T	temperature, K
T^*	non-dimensional temperature, -
u, v	velocities, $m s^{-1}$
x, y, z	coordinates, m
X, Y, Z	non-dimensional coordinates, -

Greek symbols:

λ	thermal conductivity, $Wm^{-1}K^{-1}$
μ	dynamic viscosity, Pa s
φ	heat flux, Wm^{-2}
φ_0	arbitrary heat flux, Wm^{-2}
Φ	non-dimensional heat flux, -
ρ	density, $kg m^{-3}$
σ	surface tension, $N m^{-1}$

Subscripts:

cap	capillary
eq	equivalent
l	liquid
max	maximum
s	solid
sat	saturation
v	vapour

1. Introduction

While the literature on heat pipes can be qualified as abundant, the experimental data are often difficult to compare one to the others since the geometrical properties and the experimental conditions are barely similar. Heat pipes are experimentally discriminated in terms of maximum heat transfer capability and thermal resistance. Nevertheless, these two characteristics depend on the size of both the evaporator and the condenser as well as the overall dimensions of the heat pipe. Moreover, the thermal design of a complete system (like the cooling of an electronic card and its environment) using a heat pipe to transport or spread the heat dissipated by one or several heat sources is inadequate using such characteristics. There are three fundamental parameters, associated to the capillary structure of the heat pipe¹, that enable to characterize its performance regardless of the experimental conditions: the equivalent thermal conductivity λ_{eq} , the permeability K and the maximum capillary pressure $\Delta P_{cap, max}$.

The thermal modelling of a heat pipe requires the resolution of the 3D heat transfer equation in its wall. Indeed, the heat flux is transferred both transversally through the wall and the capillary structure, where evaporation and condensation phenomena occur, but also longitudinally due to the high thermal conductivity of the material in which the heat pipe is made of. The heat transfer through the capillary structure can be assumed 1D since its equivalent thermal conductivity λ_{eq} is generally small compared to the thermal conductivity of the body and the capillary structure is usually thin, leading to a negligible longitudinal heat transfer in the capillary structure. Furthermore, the velocity of the liquid inside the capillary structure is small enough to neglect convection effects. The thermal resistance of the vapour is generally small if the vapour space is well designed, inducing a small pressure drop. Thus, its temperature can be considered as constant and equal to the saturation temperature. From a thermal point of view, apart from the geometrical properties of the heat pipe and the thickness of the capillary structure, the criterion that enables to compare two heat pipes one to the other is the equivalent thermal conductivity of the capillary structure.

The determination of the maximum heat transfer capability of a heat pipe requires the calculation of the pressure fields in both the liquid and the vapour. Since the internal thickness of the heat pipe is usually small, the fluid flows are mostly 2D. The relationship between the liquid velocity and the pressure is generally given by the Darcy's law which depends on the permeability of the capillary structure. The mass balance equation has to be solved by considering the evaporation and condensation flow rates. The latter are highly linked to the thermal model since the longitudinal heat diffusion increases the area of evaporation and condensation compare to the real surface of the heat sources and the heat sinks. For the vapour, the mass and

¹ This paper focalizes on heat pipes being internally fully covered with a capillary structure. Other kinds of heat pipes like thermosyphons, loop heat pipes or pulsating heat pipes are not considered here. Nevertheless, most of the literature results for these heat pipes are also presented in terms of thermal resistance and maximum heat transfer capability, which leads to the same difficulty to compare two heat pipes one to the other.

momentum balance equations have to be solved with the opposite phase change mass flow rates. Hydrodynamic models enable to calculate the total pressure drops in both the liquid and the vapour. These pressure drops added up with the hydrostatic pressure have to be compared to the maximum capillary pressure that the system can sustain to check if the capillary limit is not reached. From a hydrodynamic point of view, apart from the fluid thermophysical properties, the inner geometrical properties of the heat pipe and the thickness of the capillary structure, the criteria that enable to compare two heat pipes one to the other are the permeability and the maximum capillary pressure generated by the liquid inside the capillary structure.

The essence of heat pipe modelling has been presented in last paragraphs. In the literature, the heat pipe hydrodynamic performances have been described using 1D analytical models [1–3] or 1D numerical models [4,5] for simple configurations. 2D numerical models based on the Darcy's law have also been developed [6,7]. The thermal performance were calculated numerically [8,9] or analytically [10] for simple configurations by considering an equivalent thermal conductivity for the capillary structure. Transient models have also been developed [11–13]. Obviously, it is possible to increase the sophistication of the simulations. For example, in the case of grooved heat pipes, the introduction of the Young-Laplace law in the hydrodynamic model enables to describe accurately the shape of the liquid-vapour interface all along the grooves [2,14,15]. The physics of the triple line at the junction between the wall and the meniscus is also discussed in numerous studies [16–18]. Therefore, both the hydrodynamic and the thermal models can be developed using local equations based on the detailed position of the liquid, vapour and capillary structure. However, this approach is not convenient in other capillary structures (such as meshes or sintered powder wicks) due to their geometrical complexity. Therefore, the resort to the three fundamental characteristic parameters of the capillary structure is needed [19], enabling to take into account the major physical phenomena inside a heat pipe using simple equations.

Any common numerical method can be employed to solve both the hydrodynamic and the thermal models. Nevertheless, due to the 3D nature of the heat pipe and to the coupling between hydrodynamic and thermal equations, numerical methods can be time consuming. Another approach consists in solving the equation analytically, which can be considered as tricky as a first sight. Analytical solutions have been mostly forgotten nowadays since they are limited to a restricted number of geometry and are often perceived as complex. However, the simple shape of a conventional heat pipe enables to obtain solutions having a simple formalism and which are by essence accurate. Furthermore, they are particularly appropriate when several heat sources are located at any places on the heat pipe external wall.

In 2006, Lefèvre and Lallemand [20] developed an analytical solution for the 3D temperature field and the 2D pressure and velocity fields within a flat plate heat pipe. The thermal and the hydrodynamic models were coupled together. The model was able to cope with several heat sources and heat sinks located anywhere on the heat pipe, but the system was fully insulated on one of its face. In [21], the equations were improved to consider two different thermal conductivities at the evaporator and at the condenser. More recently, Aghvami and Faghri [22] proposed solutions for flat plate heat pipes, having one face covered by a

capillary structure and the other in contact with the vapour. They were able to compare various heating and cooling configurations at the bottom and the top faces of a flat plate heat pipe. In 2011, Shabgard and Faghri [23] developed analytical expressions using Bessel functions for cylindrical heat pipes.

In this paper, we show that it is possible to extend the equations of Lefèvre and Lallemand [20] to all the classical configurations of conventional heat pipes (cylindrical and fully covered flat plate heat pipe) by introducing new kinds of symmetries on the boundaries. The thermal and hydrodynamic equations are presented in the first section and in the second section of the paper respectively. In the last section, different examples are presented to highlight the capabilities of the model.

2. Thermal model

In a heat pipe, heat is transferred by conduction in the wall and by phase change at the interface between the capillary structure and the vapour. Usually, the body shape of a heat pipe, as well as its capillary structure, is either cylindrical or rectangular. Analytical solutions of this kind of thermal problem can be derived using Fourier series if the domain can be considered as periodic. It can be periodic by itself, as along the circumferential coordinate of a cylindrical heat pipe or it can be built to be periodic if adiabatic boundary conditions exist. Indeed, a domain bounded by adiabatic conditions is equivalent to a larger domain bounded by periodic conditions. The latter is created by introducing additional fictive domains that are symmetric to the initial domain with respect to the adiabatic lines. Three different heat pipe configurations are considered in this paper (Figure 1):

- Configuration A corresponds to a FPHP made of two plates fully covered internally with a capillary structure. The upper and lower faces are thermally linked, which ensures a thermal continuity - symbolized by arrows in figure 1b - on both the x and the y axes.
- Configuration B is similar to configuration A, but only one plate is covered with a capillary structure, the other plate being assumed adiabatic. Therefore, the boundaries on the x and y axes can be considered as adiabatic. The equations of this configuration were already developed in Lefèvre and Lallemand [20].
- Configuration C is a cylindrical heat pipe. Let us assume that the thickness of the body is small enough to solve the thermal problem in Cartesian coordinates. This hypothesis is realistic since the heat pipe body thickness is usually small compared to its perimeter. As a result, the heat pipe can be opened out and represented by a plate with a thermal link on the y axis. The extremities of the cylindrical heat pipe on the x axis are assumed adiabatic.

Let us introduce the non-dimensional dimensions $X = x / a$ and $Y = y / b$ where a and b are the dimensions of the heat pipe along the x and y axes respectively. The considered domain for the Fourier series is bounded by the coordinates $-1 < X < 1$ and $-1 < Y < 1$. Figure 1c summarizes the representation of the three heat pipe configurations in a periodic domain adapted to the Fourier series:

- In configuration A, the considered domain represents two times the surface of both the upper and the lower faces of the FPHP. Let us assume that the upper face is located in the surface $X > 0$ and $Y > 0$. As it is connected along its boundary $(X,0)$ and its boundary $(0,Y)$ with the lower surface, the latter has to be located in the surface $X > 0$ and $Y < 0$, but also in the surface $X < 0$ and $Y > 0$. As the lower faces are connected along their boundary $(0,-X)$ and $(0,-Y)$ with the upper face, the latter is also located in the surface $X < 0$ and $Y < 0$. Finally, the FPHP can be represented in the domain space by a symmetrical configuration, the origin $(X = 0; Y = 0)$ being the centre of symmetry.
- In configuration B, all the boundaries are adiabatic. The corresponding periodic domain can be built with two axial symmetries. It corresponds to 4 times the initial domain.
- In configuration C, the X axis represents the length of the cylindrical heat pipe, the extremities of the heat pipe ($X = 0$ and $X = 1$) being assumed adiabatic. The perimeter of the heat pipe is delimited by $-1 < Y < 1$. In the present study, b is considered to be equal to half the internal perimeter of the heat pipe. The surface defined by $X > 0$ is the total opened out surface of the heat pipe whereas the surface defined by $X < 0$ is its symmetric with respect to the Y axis.

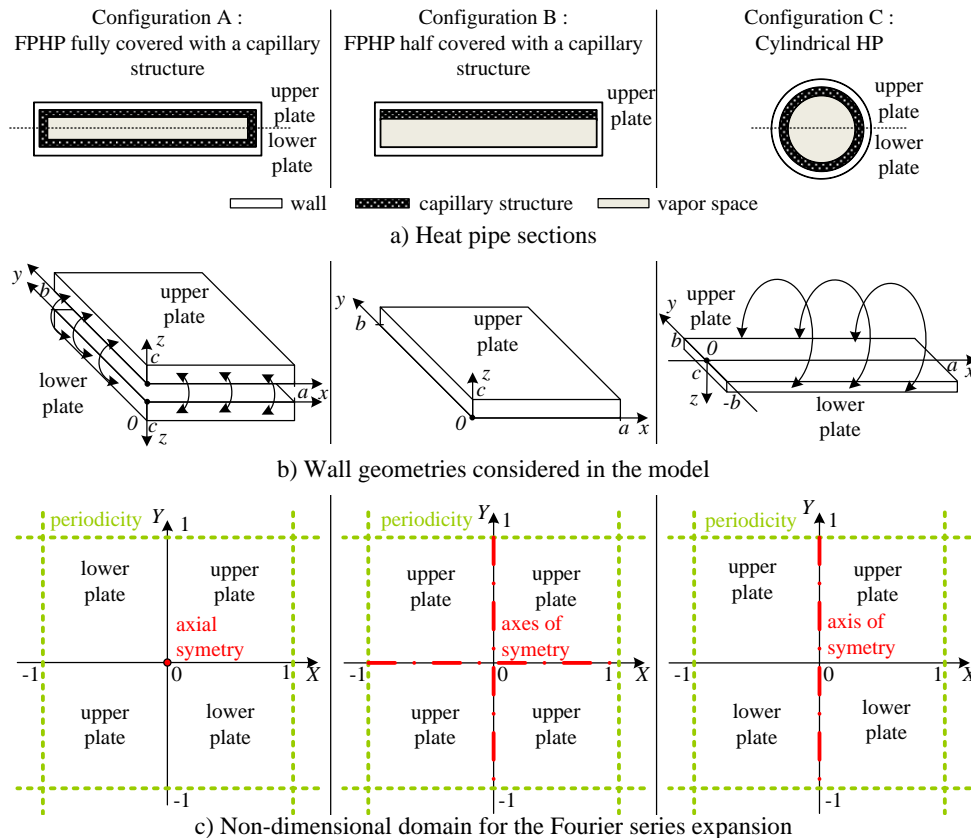


Figure 1: Geometries and corresponding domains for three heat pipe configurations

Due to the periodic representation of the domain, the 3D temperature field in the heat pipe body can be expressed as the sum of Fourier series for the three configurations. Its general form is given by [24]:

$$\begin{aligned}
T^*(X, Y, Z) = & \sum_{m=1}^{\infty} \sum_{n=1}^{\infty} A_{mn}(Z) \sin(m\pi X) \sin(n\pi Y) + \sum_{m=1}^{\infty} \sum_{n=0}^{\infty} A'_{mn}(Z) \sin(m\pi X) \cos(n\pi Y) \\
& + \sum_{m=0}^{\infty} \sum_{n=1}^{\infty} B'_{mn}(Z) \cos(m\pi X) \sin(n\pi Y) + \sum_{m=0}^{\infty} \sum_{n=0}^{\infty} B_{mn}(Z) \cos(m\pi X) \cos(n\pi Y)
\end{aligned} \tag{1}$$

Where A_{mn} , A'_{mn} , B'_{mn} and B_{mn} are functions of the non-dimensional coordinate $Z = z / c$ and c is the thickness of the heat pipe walls. T^* is the dimensionless temperature defined as:

$$T^* = \frac{\lambda_s}{\varphi_0 c} \Delta T \tag{2}$$

where $\Delta T = T - T_{sat}$ is the temperature difference between the local temperature T and the vapor temperature assumed to be constant and equal to the saturation temperature T_{sat} . λ_s is the thermal conductivity of the heat pipe body and φ_0 an arbitrary constant with the dimension of a heat flux.

The 3D heat conduction equation is solved in the heat pipe body assuming that, apart from the heat sources and the heat sinks, the external surface of the heat pipe is well insulated. Within the heat pipe, the heat transfer between the heat pipe body and the vapour through the capillary structure is calculated by considering a heat transfer coefficient h . This coefficient can be estimated using experimental data or calculated by considering the equivalent thermal conductivity of the capillary structure λ_{eq} and its thickness H_p : $h = \lambda_{eq}/H_p$. It has to be noted that it is also possible to consider two different heat transfer coefficient in the condenser and in the evaporator as it has been shown in a previous paper [6]. Using the dimensionless parameters $B = b/a$ and $C = c/a$, the 3D steady-state heat conduction equation can be written as:

$$\frac{\partial^2 T^*}{\partial X^2} + \frac{1}{B^2} \frac{\partial^2 T^*}{\partial Y^2} + \frac{1}{C^2} \frac{\partial^2 T^*}{\partial Z^2} = 0 \tag{3}$$

In the plane (X, Y) , the domain is periodic. In the direction Z , the boundary conditions are written as:

$$\left. \frac{\partial T^*}{\partial Z} \right|_{Z=0} = \frac{h c}{\lambda_s} T^* = Bi T^* \tag{4}$$

$$\left. \frac{\partial T^*}{\partial Z} \right|_{Z=1} = \Phi(X, Y) = \frac{\varphi(X, Y)}{\varphi_0} \tag{5}$$

where Bi is the Biot number and $\Phi(X, Y)$ is the non-dimensional heat flux imposed on the body external face. The non-dimensional heat flux can be expressed as the sum of the heat flux imposed by each heat sources and heat sinks, which are not necessarily uniform:

$$\Phi(X, Y) = \sum_{i=1}^{n_{source} + n_{sink}} \frac{\varphi_i(X, Y)}{\varphi_0} \tag{6}$$

Due to its periodic properties, the non-dimensional heat flux can be written using the following expression:

$$\begin{aligned}
\Phi(X, Y) = & \sum_{m=1}^{\infty} \sum_{n=1}^{\infty} \left(\sum_{i=1}^{n_{source}+n_{sink}} C_{mn}(i) \right) \sin(m\pi X) \sin(n\pi Y) \\
& + \sum_{m=1}^{\infty} \sum_{n=0}^{\infty} \left(\sum_{i=1}^{n_{source}+n_{sink}} C'_{mn}(i) \right) \sin(m\pi X) \cos(n\pi Y) \\
& + \sum_{m=0}^{\infty} \sum_{n=1}^{\infty} \left(\sum_{i=1}^{n_{source}+n_{sink}} D'_{mn}(i) \right) \cos(m\pi X) \sin(n\pi Y) \\
& + \sum_{m=0}^{\infty} \sum_{n=0}^{\infty} \left(\sum_{i=1}^{n_{source}+n_{sink}} D_{mn}(i) \right) \cos(m\pi X) \cos(n\pi Y)
\end{aligned} \tag{7}$$

where n_{source} and n_{sink} are the number of heat sources and heat sinks respectively in the domain considered for the Fourier series, which is bounded by the coordinates $-1 < X < +1$ and $-1 < Y < +1$. Every heat sources and heat sinks located on the fictive symmetric domains must be considered in the equation (7). C_{mn} , C'_{mn} , D'_{mn} and D_{mn} are the Fourier coefficient associated to each heat sources and heat sinks. Their expression depend on both the location and the heat flux of each heat sources and heat sinks [24]:

$$\begin{aligned}
C_{mn}(i) &= \iint_{source\ or\ sink} \Phi_i(X, Y) \sin(m\pi X) \sin(n\pi Y) dXdY \\
C'_{mn}(i) &= \iint_{source\ or\ sink} \Phi_i(X, Y) \sin(m\pi X) \cos(n\pi Y) dXdY \\
D'_{mn}(i) &= \iint_{source\ or\ sink} \Phi_i(X, Y) \cos(m\pi X) \sin(n\pi Y) dXdY \\
D_{mn}(i) &= \iint_{source\ or\ sink} \Phi_i(X, Y) \cos(m\pi X) \cos(n\pi Y) dXdY
\end{aligned} \tag{8}$$

For a rectangular heat source or heat sink i with a uniform heat flux $\varphi(i)$ and coordinates $[a_1(i), a_2(i), b_1(i), b_2(i)]$, these coefficients are given in appendix 1. Other geometries of heat sources and heat sinks can be considered if they can be expressed in terms of Fourier series expansion on the periodic domain.

By substituting equations (1) and (7) into equation (3) and by taking into consideration the boundary limits given by equations (4) and (5), the following expressions for the coefficients A_{mn} , A'_{mn} , B'_{mn} and B_{mn} can be found:

$$A_{mn}(Z) = \left[\sum_{i=1}^{n_{source}+n_{sink}} C_{mn}(i) \right] \frac{[(G\pi C + Bi) \exp(G\pi CZ) + (G\pi C - Bi) \exp(-G\pi CZ)]}{G\pi C [(G\pi C + Bi) \exp(G\pi C) - (G\pi C - Bi) \exp(-G\pi C)]} \tag{9}$$

$$A'_{mn}(Z) = \left[\sum_{i=1}^{n_{source}+n_{sink}} C'_{mn}(i) \right] \frac{[(G\pi C + Bi) \exp(G\pi CZ) + (G\pi C - Bi) \exp(-G\pi CZ)]}{G\pi C [(G\pi C + Bi) \exp(G\pi C) - (G\pi C - Bi) \exp(-G\pi C)]} \tag{10}$$

$$B'_{mn}(Z) = \left[\sum_{i=1}^{n_{source}+n_{sink}} D'_{mn}(i) \right] \frac{[(G\pi C + Bi) \exp(G\pi CZ) + (G\pi C - Bi) \exp(-G\pi CZ)]}{G\pi C[(G\pi C + Bi) \exp(G\pi C) - (G\pi C - Bi) \exp(-G\pi C)]} \quad (11)$$

$$B_{mn}(Z) = \left[\sum_{i=1}^{n_{source}+n_{sink}} D_{mn}(i) \right] \frac{[(G\pi C + Bi) \exp(G\pi CZ) + (G\pi C - Bi) \exp(-G\pi CZ)]}{G\pi C[(G\pi C + Bi) \exp(G\pi C) - (G\pi C - Bi) \exp(-G\pi C)]} \quad (12)$$

where

$$G = \sqrt{m^2 + \left(\frac{n}{B}\right)^2} \quad (13)$$

Because of the symmetry of the three configurations proposed in the present study, the general expression given by equations (1) and (7) can be simplified. These simplified expressions are given in the appendix 2 for each configuration. In this table, $\tilde{n}_{sources}$ and \tilde{n}_{sink} are the real number of heat sources and heat sinks in the physical domain. Even if the general formalism of the temperature field can appear as complex, the final solution for each configuration is simple. It has to be noted that the 3D temperature field of the heat pipe requires only the calculation of cosine, sine and exponential functions.

The first step of the resolution is to calculate the coefficients C_{mn} , C'_{mn} , D'_{mn} and D_{mn} knowing the coordinates and the heat flux of the heat sources and the heat sinks. The second step is to calculate the temperature of the wall at each point of the domain using equation (1). It has to be noted that in order to determine the heat pipe thermal performance, the entire temperature field does not have to be calculated. The temperature is required only at specific locations on the heat pipe, which generally correspond to the maximum and minimum temperatures. This is a huge advantage compared with a numerical model for which the whole temperature field has to be calculated even if the temperature is required only at some locations.

3. Hydrodynamic Model

In order to predict the maximum heat transfer capability of a heat pipe, the pressure drops in both the liquid and the vapour need to be calculated. Indeed, the dry-out of a fraction of the heat pipe occurs when the difference of pressure between the liquid and the vapour is higher than the maximum capillary pressure that the capillary structure can sustain. The present hydrodynamic model is based on the Darcy's law. For the liquid phase, the equations are solved on the periodic domain adapted to the Fourier series. For the vapor phase, the geometry of the domain depends on the heat pipe configuration.

3.1. Hydrodynamic model for the liquid

As the capillary structure is usually thin compared to the dimensions of the heat pipe, the liquid flow can be considered as two-dimensional for all the configurations. In Cartesian coordinates, the Darcy's law can be written as:

$$\begin{aligned}
u_l &= -\frac{K}{\mu_l} \frac{\partial P_{t,l}}{\partial x} = -\frac{K}{\mu_l} \frac{1}{a} \frac{\partial P_{t,l}}{\partial X} \\
v_l &= -\frac{K}{\mu_l} \frac{\partial P_{t,l}}{\partial y} = -\frac{K}{\mu_l} \frac{1}{b} \frac{\partial P_{t,l}}{\partial Y}
\end{aligned} \tag{14}$$

where u_l and v_l are the liquid velocity components along the x and y axes respectively. K is the permeability of the capillary structure. It has to be noted that it is also possible to consider an anisotropic case with K_1 and K_2 the permeabilities along the x and y directions respectively. $P_{t,l}$ is the total pressure of the liquid. Neglecting the dynamic pressure, it can be written as the sum of the liquid pressure and the gravitational head:

$$P_{t,l}(X, Y) = P_l(X, Y) + \rho g h_l(X, Y) \tag{15}$$

where h_l is the altitude of the capillary structure at the coordinates (X, Y) .

The Darcy's law is convenient for analytical resolution since it leads to a linear differential equation for the pressure field. As a consequence, the Fourier series expansion is well adapted for its resolution. In some numerical works, the equations for the porous media are more complex but they lead to a nonlinear formulation that prevents them to be used in an analytical formulation. The boundary conditions of the hydrodynamic model are similar to that of the thermal model. In configuration A, the lower and upper plates are hydrodynamically linked. In configuration B, the velocities along the axes perpendicular to the symmetry axes are equal to zero. In configuration C, a hydrodynamic link exists along the y direction, while the velocity component along the x direction is equal to zero at both extremities. This condition is verified by the symmetry properties of the periodic domain.

The mass balance can be written as:

$$\frac{\partial u_l}{\partial X} + \frac{1}{B} \frac{\partial v_l}{\partial Y} = \frac{-(-\varphi|_{z=0})a}{h_{lv}\rho_l H_p} \tag{16}$$

where h_{lv} is the latent heat of vaporization of the working fluid. $\varphi|_{z=0}$ is the heat flux at the liquid-vapor interface. It can be expressed as a function of the temperature field, calculated by the thermal model:

$$\varphi|_{z=0} = -\varphi_0 Bi T^*|_{z=0} \tag{17}$$

By considering equations (14) to (17), the differential equation to be solved can be expressed as:

$$\frac{\partial^2 P_{t,l}}{\partial X^2} + \frac{1}{B^2} \frac{\partial^2 P_{t,l}}{\partial Y^2} = \frac{a^2 \mu_l \varphi_0 Bi}{KH_p h_{lv} \rho_l} T^*|_{z=0} \tag{18}$$

On the periodic domain, the liquid pressure field can be expressed with the same form as the temperature field (equation (1)). By introducing the expression of $T^*|_{z=0}$ in equation (18), the total pressure field of the liquid can be written:

$$\begin{aligned}
P_{t,l}(X, Y) = & -\frac{a^2 \mu_l \varphi_0 Bi}{\pi^2 K H_p h_{lv} \rho_l} \left[\sum_{m=1}^{\infty} \sum_{n=1}^{\infty} \frac{A_{mn}(0)}{G^2} \sin(m\pi X) \sin(n\pi Y) \right. \\
& + \sum_{m=1}^{\infty} \sum_{n=0}^{\infty} \frac{A'_{mn}(0)}{G^2} \sin(m\pi X) \cos(n\pi Y) + \sum_{m=0}^{\infty} \sum_{n=1}^{\infty} \frac{B'_{mn}(0)}{G^2} \cos(m\pi X) \sin(n\pi Y) \\
& \left. + \sum_{m=0}^{\infty} \sum_{n=0}^{\infty} \frac{B_{mn}(0)}{G^2} \cos(m\pi X) \cos(n\pi Y) \right] \quad (19)
\end{aligned}$$

The pressure field is defined up to a constant. The expressions of the liquid velocity can be obtained by introducing equation (19) into equation (14):

$$\begin{aligned}
u_l(X, Y) = & \frac{a \varphi_0 Bi}{\pi H_p h_{lv} \rho_l} \left[\sum_{m=1}^{\infty} \sum_{n=1}^{\infty} \frac{mA_{mn}(0)}{G^2} \cos(m\pi X) \sin(n\pi Y) \right. \\
& + \sum_{m=1}^{\infty} \sum_{n=0}^{\infty} \frac{mA'_{mn}(0)}{G^2} \cos(m\pi X) \cos(n\pi Y) \\
& - \sum_{m=0}^{\infty} \sum_{n=1}^{\infty} \frac{mB'_{mn}(0)}{G^2} \sin(m\pi X) \sin(n\pi Y) \\
& \left. - \sum_{m=0}^{\infty} \sum_{n=0}^{\infty} \frac{mB_{mn}(0)}{G^2} \sin(m\pi X) \cos(n\pi Y) \right] \quad (20)
\end{aligned}$$

$$\begin{aligned}
v_l(X, Y) = & \frac{a^2 \varphi_0 Bi}{b \pi H_p h_{lv} \rho_l} \left[\sum_{m=1}^{\infty} \sum_{n=1}^{\infty} \frac{nA_{mn}(0)}{G^2} \sin(m\pi X) \cos(n\pi Y) \right. \\
& - \sum_{m=1}^{\infty} \sum_{n=0}^{\infty} \frac{nA'_{mn}(0)}{G^2} \sin(m\pi X) \sin(n\pi Y) \\
& + \sum_{m=0}^{\infty} \sum_{n=1}^{\infty} \frac{nB'_{mn}(0)}{G^2} \cos(m\pi X) \cos(n\pi Y) \\
& \left. - \sum_{m=0}^{\infty} \sum_{n=0}^{\infty} \frac{nB_{mn}(0)}{G^2} \cos(m\pi X) \sin(n\pi Y) \right] \quad (21)
\end{aligned}$$

As for the temperature field, the solutions presented in the appendix 2 can be used to simplify the expressions of the pressure and velocity fields in the liquid.

3.2. Hydrodynamic model for the vapour

The geometry of the vapour channel depends on the heat pipe configuration. It can be parallelepipedic for the configuration A and B, or cylindrical for the configuration C. However, for all configurations, an approach similar to the liquid phase is used to calculate the vapour pressure and velocity fields in the heat pipe.

3.2.1. Configuration A

In configuration A, the vapour flow can be considered as a laminar flow between the two parallel plates. In these conditions, it is possible to link the velocity and the pressure fields:

$$\begin{aligned} u_v &= -\frac{H_v^2}{12a\mu_v} \frac{\partial P_v}{\partial X} \\ v_v &= -\frac{H_v^2}{12b\mu_v} \frac{\partial P_v}{\partial Y} \end{aligned} \quad (22)$$

where H_v is the vapor space thickness. The dynamic pressure and the gravitational head are neglected for the vapor phase. The mass balance for the vapor space can be expressed as:

$$\frac{\partial u_v}{\partial X} + \frac{1}{B} \frac{\partial v_v}{\partial Y} = \frac{-(\varphi(X, Y)|_{z=0} + \varphi(-X, Y)|_{z=0})a}{h_{lv}\rho_v H_v} \quad (23)$$

This equation takes into account the evaporation or condensation mass fluxes coming from both the lower and the upper plates. The mass flux can be expressed by means of the temperature field:

$$\varphi(X, Y)|_{z=0} + \varphi(-X, Y)|_{z=0} = -\varphi_0 Bi (T^*(X; Y) + T^*(-X; Y))|_{z=0} \quad (24)$$

The differential equation to be solved becomes :

$$\frac{\partial^2 P_v}{\partial X^2} + \frac{1}{B^2} \frac{\partial^2 P_v}{\partial Y^2} = -\frac{12\mu_v a^2 \varphi_0 Bi}{H_v^3 h_{lv} \rho_v} (T^*(X; Y) + T^*(-X; Y))|_{z=0}$$

This equation has to be solved for $0 < X < l$ and $0 < Y < l$. By considering the expression of equation (1) in configuration A, we obtain:

$$T^*(X; Y) + T^*(-X; Y) = 2 \sum_{m=0}^{\infty} \sum_{n=0}^{\infty} B_{mn}(Z) \cos(m\pi X) \cos(n\pi Y) \quad (26)$$

Eventually, the vapour pressure and velocity fields can be expressed in terms of Fourier series:

$$P_v(X, Y) = \frac{24a^2 \mu_v \varphi_0 Bi}{\pi^2 H_v^3 h_{lv} \rho_v} \sum_{m=0}^{\infty} \sum_{n=0}^{\infty} \frac{B_{mn}(0)}{G^2} \cos(m\pi X) \cos(n\pi Y) \quad (27)$$

$$u_v(X, Y) = \frac{2a\varphi_0 Bi}{\pi H_v h_{lv} \rho_v} \sum_{m=0}^{\infty} \sum_{n=0}^{\infty} \frac{m B_{mn}(0)}{G^2} \sin(m\pi X) \cos(n\pi Y) \quad (28)$$

$$v_v(X, Y) = \frac{2a^2 \varphi_0 Bi}{b\pi H_v h_{lv} \rho_v} \sum_{m=0}^{\infty} \sum_{n=0}^{\infty} \frac{n B_{mn}(0)}{G^2} \cos(m\pi X) \sin(n\pi Y) \quad (29)$$

3.2.1. Configuration B

The configuration B is close to the configuration A, but the lower plate is free of capillary structure. Thus, evaporation and condensation mass fluxes come only from the upper plate. The mass balance becomes:

$$\frac{\partial u_v}{\partial X} + \frac{1}{B} \frac{\partial v_v}{\partial Y} = \frac{-\varphi|_{z=0} a}{h_{lv} \rho_v H_v} \quad (30)$$

As a consequence, the vapour pressure and velocity expressions are:

$$P_v(X, Y) = \frac{12a^2 \mu_v \varphi_0 Bi}{\pi^2 H_v^3 h_{lv} \rho_v} \sum_{m=0}^{\infty} \sum_{n=0}^{\infty} \frac{B_{mn}(0)}{G^2} \cos(m\pi X) \cos(n\pi Y) \quad (31)$$

$$u_v(X, Y) = \frac{a \varphi_0 Bi}{\pi H_v h_{lv} \rho_v} \sum_{m=0}^{\infty} \sum_{n=0}^{\infty} \frac{m B_{mn}(0)}{G^2} \sin(m\pi X) \cos(n\pi Y) \quad (32)$$

$$v_v(X, Y) = \frac{a^2 \varphi_0 Bi}{b \pi H_v h_{lv} \rho_v} \sum_{m=0}^{\infty} \sum_{n=0}^{\infty} \frac{n B_{mn}(0)}{G^2} \cos(m\pi X) \sin(n\pi Y) \quad (33)$$

Solutions have to be calculated for $0 < X < l$ and $0 < Y < l$.

3.2.2. Configuration C

In the configuration C, the vapour space is cylindrical. The vapour flow is assumed to be one dimensional along the X axis. Under this assumption, the pressure drop can be linked to the vapour velocity through:

$$u_v = -\frac{d^2}{32\mu_v} \frac{1}{a} \frac{dP_v}{dX} \quad (34)$$

The mass balance equation can be written as:

$$\frac{du_v}{dX} = 4 \frac{a}{d} u_{evap} \quad (35)$$

with u_{evap} the phase change velocity at the liquid vapor interface. As $b = \pi d/2$, u_{evap} can be calculated by integration of the heat flux along the perimeter of the heat pipe:

$$u_{evap} = \frac{1}{\rho_v h_{lv}} \frac{b}{\pi d} \int_{Y=-1}^1 \varphi(X, Y)|_{z=0} dY = \frac{1}{2} \frac{\varphi_0 Bi}{\rho_v h_{lv}} \int_{Y=-1}^1 T^*(X, Y)|_{z=0} dY \quad (36)$$

By introducing equations (34) and (36) into equation (35), the governing differential equation becomes:

$$\frac{d^2 P_v}{dX^2} = -\frac{64a^2 \mu_v \varphi_0 Bi}{d^3 h_{lv} \rho_v} \int_{Y=-1}^1 T^*(X, Y)|_{z=0} dY \quad (37)$$

Due to the geometry of the domain, we also get:

$$\int_{Y=-1}^1 T^*(X, Y)|_{z=0} dY = 2 \sum_{n=0}^{\infty} B_{m0}(0) \cos(m\pi X) \quad (38)$$

Eventually, the vapour pressure and velocity expressions are:

$$P_v(X) = \frac{128a^2 \mu_v \varphi_0 Bi}{\pi^2 d^3 h_{lv} \rho_v} \sum_{m=0}^{\infty} \frac{B_{m0}(0)}{m^2} \cos(m\pi X) \quad (39)$$

$$u_v(X) = \frac{4a\varphi_0 Bi}{\pi d h_{lv} \rho_v} \sum_{m=0}^{\infty} \frac{B_{m0}(0)}{m} \sin(m\pi X) \quad (40)$$

Solutions have to be calculated for $0 < X < 1$.

3.3. Calculation of the hydrodynamic performance

The maximum heat transfer capability of a heat pipe is governed by several limitations that must be addressed when designing a heat pipe. These heat transport limits are named the viscous, sonic, capillary pumping, entrainment and boiling limits. They are functions of the heat pipe operating temperature. Except the boiling limit that can be calculated using the thermal model, the determination of the other limits requires either the pressure or the velocity fields inside both the liquid and the vapour. Thus, the hydrodynamic model can be used to cope with the determination of these limits, as soon as the liquid and vapour flows can be considered as laminar in the liquid and the vapour, which is mostly the case in a conventional heat pipe.

The main limit that has to be considered when designing a heat pipe is the capillary pumping, which is linked to the capillary pressure. The latter is the difference between the vapour and the liquid pressure at any point of the liquid-vapour interface. This pressure difference is balanced by the capillary forces:

$$P_{\text{cap}} = P_v - P_l = \frac{2\sigma}{r} \quad (41)$$

where r is the radius of curvature of the liquid-vapour interface. If the calculated capillary pressure is higher than the maximum capillary pressure that the capillary structure can sustain, a dry-out occurs, which leads to the decrease of the thermal performance of the heat pipe. However, as the liquid and vapour pressure fields are defined up to a constant in the hydrodynamic model, the capillary pressure is also defined up to a constant by the model. The usual assumption made in the literature is to consider a flat liquid-vapour interface at the condenser. In the analytical model, it consists in setting the capillary pressure to zero for the point where the difference of pressure between the vapour and the liquid is minimal.

As for the thermal model, it is not necessary to calculate the pressure and velocity fields on the entire surface but only at the points that are necessary to estimate the hydrodynamic performance.

4. Model applications

The equations of the model were validated by comparison with experimental data in the case of configuration B in the paper of Lefèvre and Lallemand [20]. For the same configuration, Sonan et al [13] compared their transient 3D numerical model to the same equations and found also a good agreement. Furthermore, in section 4.3, the equations are derived in the case of the classical problem involving cylindrical heat pipes heated on one side and cooled on the other side. We show that the simplification enables to establish the well-known theory of heat pipe modelling, which also validates the proposed approach. In practice, the analytical model can be used mainly for three different goals:

- the prediction of the thermal and hydrodynamic heat pipe performances,
- the prediction of the capillary structure properties from experimental results,
- the derivation of simple and straightforward analytical expressions of the working limits.

Several examples are presented in this section to illustrate each of these possible applications.

4.1. Prediction of the thermal and hydrodynamic heat pipe performances

The analytical model can predict the thermal and hydrodynamic behaviour of a conventional heat pipe in many applications. As an example, the modelling of a FPHP used for the cooling of several electronic components is considered in order to highlight its capabilities and its limits. In this example, the thermal conductivity of an electronic card is improved using a flat plate heat pipe inserted directly inside the printed circuit board (PCB). The card is connected to the housing of an electronic package using thermal wedgelocks as shown in figure 2. Therefore, the heat dissipated by the electronic components is transferred to the housing first by the FPHP and finally through the thermal wedgelocks. Then the heat spreads inside the housing, which is cooled down by natural convection of air. This configuration is similar to the experimental work presented in [25]. The surface of the FPHP in contact with the two thermal wedgelocks corresponds to the location of the heat sinks. In the analytical model, we assume that the heat dissipated by the components is equally distributed on both heat sinks. Several electronic components can be located on the top and on the bottom parts of the FPHP. In the present study, three electronic components are considered. The dimensions and the different parameters of the study are summarized in table 1 and table 2. A capillary structure made of crossed grooves is considered, as presented in [26].

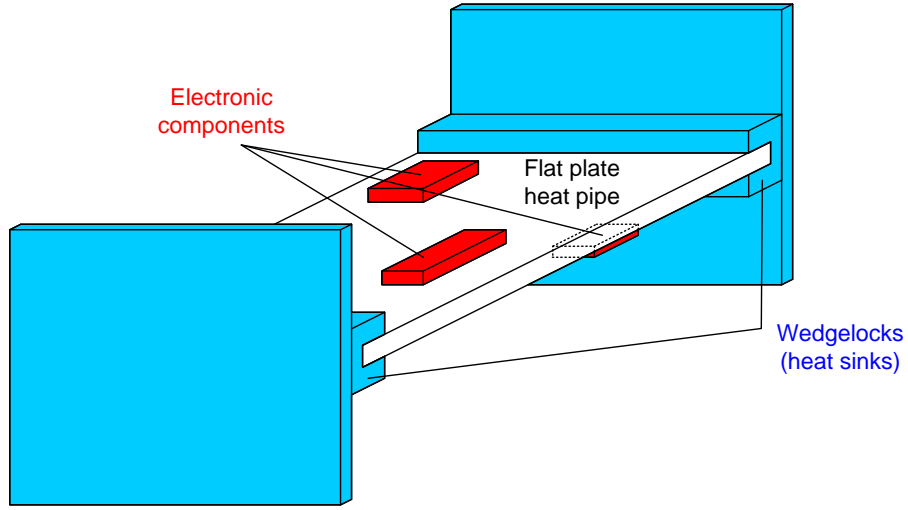


Figure 2: Geometry of the FPHP for the cooling of multiple electronic components

Table 1: FPHP dimensions and properties

Flat plate heat pipe	
Length a	0.3 m
Width b	0.15 m
Wall thickness c	1 mm
Wall conductivity λ_s	380 W/mK
Vapour space H_v	1.6 mm
Capillary structure	
Thickness H_p	400 μm
Thermal conductivity λ_{eq}	1 W/mK
Permeability K	10^{-9} m^2
Effective pore radius	200 μm
Fluid	
Water	
Saturation temperature	40°C

Table 2: Coordinates and heat transfer rate of the heat sources and heat sinks

Coordinates & Q	Source 1	Source 2	Source 3	Sink 1	Sink 2
a_1/a (-)	0.2	0.4	0.5	0	0.967
a_2/a (-)	0.3	0.7	0.7	0.033	1
b_1/b (-)	0.1	0.6	-0.7	-1	-1
b_2/b (-)	0.4	0.8	-0.5	1	1
Q (W)	60	40	40	70	70

The representation of the FPHP in the physical domain is presented in figure 3 (a). The upper and lower plates of the FPHP are represented for $y > 0$ and $y < 0$ respectively. The location of the heat sources and heat sinks are highlighted in dashed lines. The representation of the problem in the non-dimensional domain for the Fourier transformation is presented in figure 3 (b). It corresponds to the configuration A: the top and the bottom plates are thermally linked through their four edges.

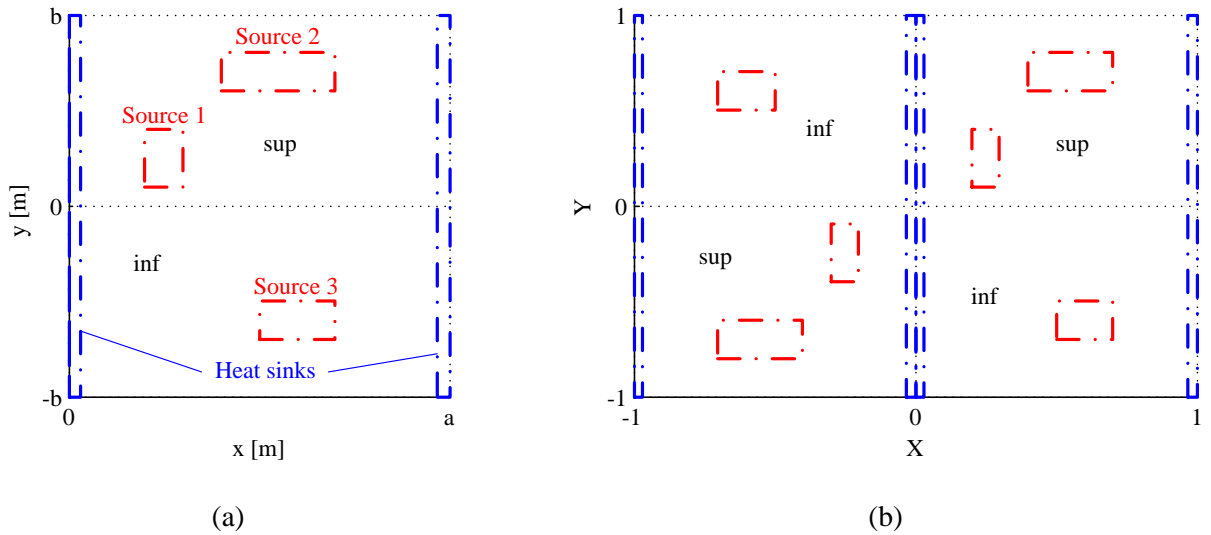


Figure 3: Physical domain (a) and non-dimensional domain for the Fourier transformation (b)

Figure 4 presents the temperature field inside the wall of the FPHP. As the wall is thin and its thermal conductivity is high, the temperature variation is negligible along the z axis. The temperature gradients are very large near the sources and flat elsewhere which shows the spreading effect of the heat pipe. The maximum temperature is reached at the location of source 1, which has the highest power. The hydrodynamic model enables to calculate the liquid velocity in the capillary structure (figure 5), the vapour velocity in the vapour space (figure 6) and the capillary pressure field (figure 7). The results clearly show the 2D nature of the flow inside the heat pipe.

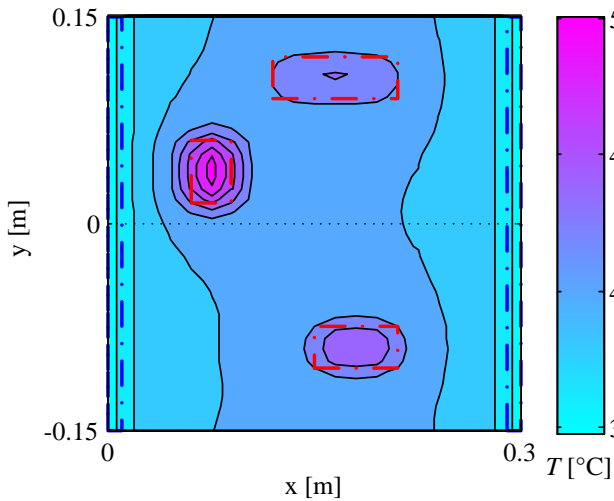


Figure 4: Wall temperature field

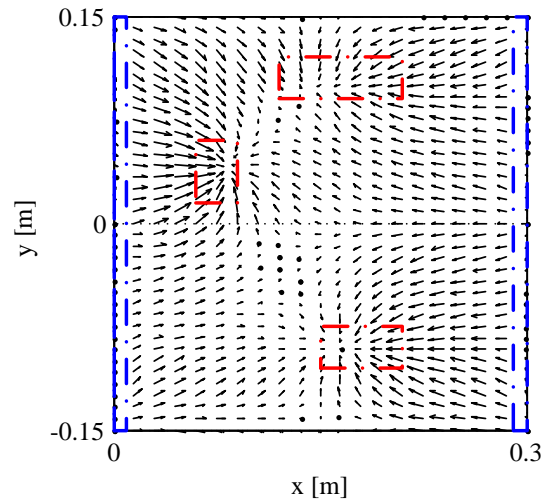


Figure 5: Liquid velocity field
($u_{\max} = 3.7 \cdot 10^{-4} \text{ m/s}$)

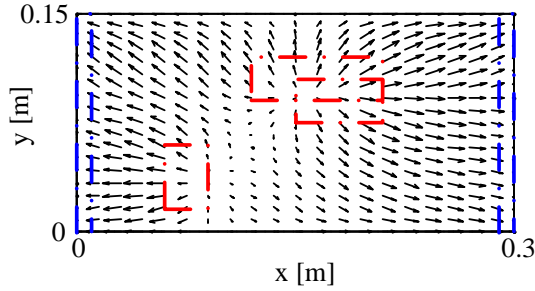


Figure 6: Vapour velocity field
($u_{\max} = 2.95$ m/s)

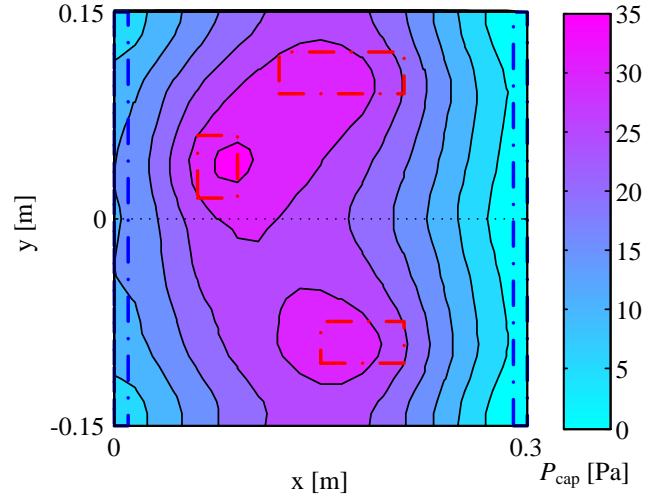


Figure 7: Capillary pressure field

Figure 4 to figure 7 highlight the thermal and hydrodynamic continuity between the top and the bottom plates. The maximum of the capillary pressure is reached at the level of the heat sources. It is equal to 35 Pa, which is much lower than the maximum capillary pressure generated by this type of heat pipes [26]. Thus, the dry-out will not occur in these conditions.

The analytical model enables to solve the thermal and hydrodynamic equations involved in a heat pipe with a low computation time. As a consequence, it could easily be used to optimize the location of the heat sources on the electronic card by considering the different constraints of the users. This type of problem can indeed be time consuming using a numerical approach.

As the boundary condition has to be homogeneous to solve the heat transfer equation analytically, the heat sinks have to be modelled by considering an imposed heat flux, which is a limit of the model. Nevertheless, if the size of the heat sink is small compared to the size of the heat pipe and the temperature of the different heat sink is the same, this assumption is reasonable.

4.2. Estimation of the properties of the capillary structure by comparison with experimental data

The determination of the heat pipe performance using numerical or analytical models can be achieved only if the properties of the capillary structure are known. In practice, many models are available to calculate the permeability or the equivalent thermal conductivity of different kind of capillary structure [19], but their accuracy is most of the time very small [21]. Thus, it can be useful to estimate these properties using heat pipe experimental measurements. In this goal, using an analytical model is unquestionably relevant. As the model is analytical, it can be straightforwardly derived in an inverse formulation in order to estimate the unknown parameters by comparison with the experimental results. Compared to numerical methods, it is not necessary to calculate the whole pressure and temperature fields to obtain the solution, but just the solution at the location of the sensors. Thus, the time required for the estimation process is incomparably smaller.

Estimations of the capillary structure properties have already been presented in previous works using the model of Lefèvre and Lallemand [20] in the case of configuration B. This approach was efficient to estimate the properties of longitudinal grooves [27], crossed grooves [26] and metallic meshes [28]. The present analytical model enables the generalization of this approach for other heat pipe configurations.

4.3. Expressions of the working limits for a cylindrical heat pipe

The analytical model can also be used to give direct and easy-to-use expressions of the heat pipe performances in simple configurations. The case of a cylindrical heat pipe in a 1D configuration is considered here as an example. The heat source and the heat sink are located at each extremity of the heat pipe (figure 8). The geometry of the heat pipe is defined by its length L , its diameter d , the wall thickness c , the heat source length L_{evap} and heat sink length L_{cond} . We assume that the heat pipe is perfectly insulated, thus the heat transfer rate Q is equal at the evaporator and at the condenser.

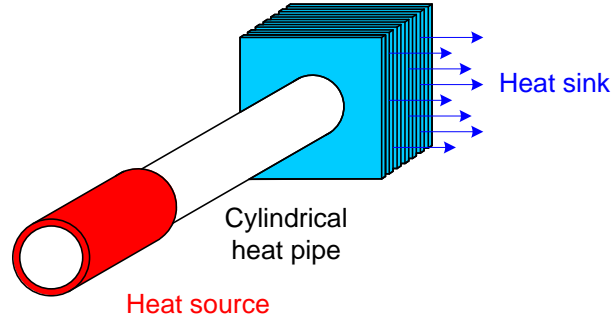


Figure 8: Heat pipe geometry

Using the Fourier series expansion, the heat flux at the outside boundary of the heat pipe can be written:

$$\varphi(X, Y) = \frac{Q}{\pi d L} \sum_{m=1}^{\infty} \frac{2}{m\pi} \left(\frac{L}{L_{evap}} \sin\left(m\pi \frac{L_{evap}}{L}\right) + \frac{L}{L_{cond}} \sin\left(m\pi \frac{L - L_{cond}}{L}\right) \right) \cos(m\pi X) \quad (42)$$

Using equations (9) to (12), the following expression can be derived for the heat pipe wall temperature:

$$T(X, Y, Z) = T_{sat} + \frac{Qc}{\pi d L \lambda_s} \sum_{m=1}^{\infty} B_{m0}(Z) \cos(m\pi X) \quad (43)$$

with:

$$B_{m0}(Z) = \frac{2}{m^2 \pi^2 C} \left[\frac{L}{L_{evap}} \sin\left(m\pi \frac{L_{evap}}{L}\right) + \frac{L}{L_{cond}} \sin\left(m\pi \frac{L - L_{cond}}{L}\right) \right] \times \frac{(m\pi C + Bi)e^{m\pi CZ} + (m\pi C - Bi)e^{-m\pi CZ}}{(m\pi C + Bi)e^{m\pi C} - (m\pi C - Bi)e^{-m\pi C}} \quad (44)$$

C being equal to c/L .

As it was discussed in the introduction, the performances of a heat pipe are generally characterized by global criteria like the overall thermal resistance R_{th} or the capillary limit $\dot{Q}_{max,cap}$ rather than the temperature and pressure fields. The temperature field expression enables to calculate directly the heat pipe thermal resistance, $R_{th} = (T_{max} - T_{min})/Q$:

$$R_{th} = \frac{c}{\pi d L \lambda_s} \sum_{m=1}^{\infty} B_{m0}(1) [1 - \cos(m\pi)] \quad (45)$$

Similarly, simple analytical expressions of the liquid and vapour pressures can be derived to calculate the capillary pressure P_{cap} :

$$P_{cap}(X) = \frac{LQBi}{\pi^3 d h_{lv}} \left[\frac{128\mu_v}{d^3 \rho_v} + \frac{\mu_l}{KH_p \rho_l} \right] \sum_{m=0}^{\infty} \frac{B_{m0}(0)}{m^2} [\cos(m\pi X) - \cos(m\pi)] \quad (46)$$

The heat pipe capillary limit is reached when the capillary pressure is equal to $2\sigma/r_{eff}$, r_{eff} being the effective pore radius of the capillary structure:

$$P_{cap,max} = \frac{L\dot{Q}_{max,cap}Bi}{\pi^3 d h_{lv}} \left[\frac{128\mu_v}{d^3 \rho_v} + \frac{\mu_l}{KH_p \rho_l} \right] \sum_{m=1}^{\infty} \frac{B_{m0}(0)}{m^2} [1 - \cos(m\pi)] = \frac{2\sigma}{r_{eff}} \quad (47)$$

As a result, the heat pipe capillary limit $\dot{Q}_{max,cap}$ can be written as:

$$\dot{Q}_{max,cap} = \frac{2\sigma h_{lv} \pi d}{r_{eff} L_{eff} \left[\frac{128\mu_v}{d^3 \rho_v} + \frac{\mu_l}{KH_p \rho_l} \right]} \times \frac{\pi^2 L_{eff}}{LBi \sum_{k=1}^{\infty} \frac{B_{(2k+1)0}(0)}{(2k+1)^2}} \quad (48)$$

with $L_{eff} = L - 0.5(L_{evap} + L_{cond})$. This expression is the product of two terms. The first term corresponds to the well-known analytical expression of the capillary limit when the heat conduction in the wall is neglected [19]. The second term is a correction factor that takes into account the heat transferred from the heat source to the heat sink by conduction in the wall. This term is always higher than 1 and is equal to 1 when the wall thickness c is equal to 0. Note that this expression is easy to calculate since the infinite sum involved in the second term converges as x^{-3} . Therefore, taking into account only the first three odd terms of the series leads to an error lower than 1%.

Similar expressions can be obtained for the other working limits since they depend either on the pressure, the velocity or the temperature. One of the main advantages of the present analytical model is to provide straightforward expressions for the heat pipe performances, taking into account the heat conduction in the heat pipe wall and the liquid and vapour flows. It has to be noted that the geometry of the present configuration is very simple but similar expressions can be obtained for much complex geometries.

Conclusion

A thermal and hydrodynamic analytical model of conventional heat pipes has been developed. The model is able to take into account various configurations such as flat plate heat pipes or cylindrical heat pipes. The capillary structure is characterized by its equivalent thermal conductivity, its permeability and the maximum capillary pressure that it can sustain. Several heat sources and heat sinks can be located anywhere on the heat pipe. The 3D heat conduction in the heat pipe wall is considered as well as the 2D liquid flow in the capillary structure. The vapour flow can be 1D or 2D depending on the configuration. Equations are solved analytically by means of a Fourier transformation which enables to have an exact solution.

As the boundary conditions have to be homogeneous to solve the heat transfer equation analytically, the heat sinks have to be modelled by considering an imposed heat flux, which is a limit of the model. Nevertheless, if the size of the heat sinks is small compared to the size of the heat pipe and the temperature of the different heat sink is the same, this assumption is reasonable. The capillary structure properties are supposed to be uniform along the heat pipe. Under certain conditions, it is possible to overcome this problem by considering different thermal conductivity on the condensation and on the evaporation zones [21]. Furthermore two different permeabilities can be considered along the x and y axis. However, neither the flooding of the system nor a partial dry-out can be taken into account.

Despite these limits, the model can be used to design a heat pipe or to model its behaviour in a real application. It can also be used to optimize the heat sources and heat sinks locations on an electronic card. As the model is analytical, the optimization process is very fast. The solution being exact, it is an efficient tool to validate a numerical model. It can also be used through an inverse approach to estimate the fundamental parameters of capillary structure by comparison with experimental data.

References

- [1] G.E. Schneider, R. Devos, Non-dimensional analysis for the heat transport capability of axially grooved heat pipes including liquid/vapor interaction, AIAA Paper N° 80-0214. (1980).
- [2] D. Khurstalev, A. Faghri, Coupled liquid and vapor flow in miniature passages with micro grooves, J. Heat Transfer. 121 (1999) 729–733.
- [3] C. Perret, Y. Avenas, C. Gillot, J. Boussey, C. Schaeffer, Integrated cooling devices in silicon technology, EPJ Applied Physics. 18 (2002) 115–124.
- [4] J.P. Longtin, B. Badran, F.M. Gerner, A one-dimensional model of a micro heat pipe during steady-state operation, J. Heat Transfer. 116 (1994) 709–715.
- [5] Y. Wang, G. Peterson, Analysis of wire-bonded micro heat pipe arrays, J. Thermophys. Heat Transfer. 16 (2002) 346–355.
- [6] N. Zhu, K. Vafai, Vapor and liquid flow in an asymmetrical flat plate heat pipe : a three-dimensional analytical and numerical investigation, Int. J. Heat Mass Transfer. 41 (1998) 159–174.
- [7] Z.J. Zuo, M.T. North, Improved heat pipe performance using graded wick structures, 11th IHPC, Musashinoshi Tokyo, Sept. 12-16. 2 (1999) 80–84.
- [8] A.K. Mallik, G.P. Peterson, Steady-state investigation of vapor deposited micro heat pipe arrays, J. Electron. Packag. 117 (1995) 75–81.
- [9] B. Xiao, A. Faghri, A three-dimensional thermal-fluid analysis of flat heat pipes, Int. J. Heat Mass Transfer. 51 (2008) 3113–3126.

- [10] B. Suman, P. Kumar, An analytical model for fluid flow and heat transfer in a micro-heat pipe of polygonal shape, *Int. J. Heat Mass Transfer*. 48 (2005) 4498–4509.
- [11] W.S. Chang, G.T. Colwell, Mathematical modeling of the transient operating characteristics of a low-temperature heat pipe, *Numerical Heat Transfer*. 8 (1985) 169–186.
- [12] G. Carbajal, C.B. Sobhan, G.P. Peterson, D.T. Queheillalt, H.N.G. Wadley, Thermal response of a flat heat pipe sandwich structure to a localized heat flux, *International Journal of Heat and Mass Transfer*. 49 (2006) 4070–4081.
- [13] R. Sonan, S. Harmand, J. Pellé, D. Leger, M. Fakès, Transient thermal and hydrodynamic model of flat heat pipe for the cooling of electronics components, *Int. J. Heat Mass Transfer*. 51 (2008) 6006–6017.
- [14] S.J. Kim, J. Ki Seo, K. Hyung Do, Analytical and experimental investigation on the operational characteristics and the thermal optimization of a miniature heat pipe with a grooved wick structure, *Int. J. Heat Mass Transfer*. 46 (2003) 2051–2063.
- [15] F. Lefèvre, R. Rullière, G. Pandraud, M. Lallemand, Prediction of the temperature field in two-phase heat spreaders with microgrooves – Experimental validation, *Int. J. Heat Mass Transfer*. 51 (2008) 4083–4094.
- [16] P.C. Wayner, A constant heat flux model of the evaporating interline region, *Int. J. Heat Mass Transfer*. 21 (1978) 362–364.
- [17] V.S. Nikolayev, Dynamics of the triple contact line on the non-isothermal heater, *J. Fluid Mech.* (2007).
- [18] R. Bertossi, Z. Lataoui, V. Ayel, C. Romestant, Y. Bertin, Modeling of Thin Liquid Film in Grooved Heat Pipes, *Numerical Heat Transfer, Part A: Applications*. 55 (2009) 1075–1095.
- [19] A. Faghri, *Heat Pipe Science And Technology*, 1st ed., Taylor & Francis, 1995.
- [20] F. Lefèvre, M. Lallemand, Coupled thermal and hydrodynamic models of flat micro heat pipes for the cooling of multiple electronic components, *Int. J. Heat Mass Transfer*. 49 (2006) 1375–1383.
- [21] R. Revellin, R. Rullière, F. Lefèvre, J. Bonjour, Experimental validation of an analytical model for predicting the thermal and hydrodynamic capabilities of flat micro heat pipes, *Appl. Therm. Eng.* 29 (2009) 1114–1122.
- [22] M. Aghvami, A. Faghri, Analysis of flat heat pipes with various heating and cooling configurations, *Applied Thermal Engineering*. 31 (2011) 2645–2655.
- [23] H. Shabgard, A. Faghri, Performance characteristics of cylindrical heat pipes with multiple heat sources, *Applied Thermal Engineering*. 31 (2011) 3410–3419.
- [24] H.S. Carslaw, J.C. Jaeger, *Conduction of heat in solids*, Clarendon Press ; Oxford University Press, 1959.
- [25] F. Lefèvre, J.-B. Conrardy, M. Raynaud, J. Bonjour, Experimental investigations of flat plate heat pipes with screen meshes or grooves covered with screen meshes as capillary structure, *Appl. Therm. Eng.* 37 (2012) 95–102.
- [26] S. Lips, F. Lefèvre, J. Bonjour, Thermohydraulic Study of a Flat Plate Heat Pipe by Means of Confocal Microscopy: Application to a 2D Capillary Structure, *J. Heat Transfer*. 132 (2010) 019008.
- [27] S. Lips, F. Lefevre, J. Bonjour, Investigation of evaporation and condensation processes specific to grooved flat heat pipes., *Frontiers in heat pipes*. 1 (2010) 023001–1 ; 023001–8.
- [28] F. Lefèvre, S. Lips, R. Rullière, J.-B. Conrardy, M. Raynaud, J. Bonjour, Flat plate heat pipes: from observations to the modeling of the capillary structure, *Frontiers in Heat Pipes*. 3 (2012).

Appendix 1: Expressions of the coefficients C_{mn} , C'_{mn} , D'_{mn} and D_{mn} for a rectangular heat source or heat sink i with a uniform heat flux $\varphi(i)$ and delimited by the coordinates $[a_1(i), a_2(i), b_1(i), b_2(i)]$

$$C_{mn}(i) = \frac{\varphi(i)}{\varphi_0} \frac{1}{mn\pi^2} \left\{ \cos\left(\frac{m\pi a_2(i)}{a}\right) - \cos\left(\frac{m\pi a_1(i)}{a}\right) \right\} \left\{ \cos\left(\frac{n\pi b_2(i)}{b}\right) - \cos\left(\frac{n\pi b_1(i)}{b}\right) \right\} \quad (49)$$

$$C'_{mn}(i) = -\frac{\varphi(i)}{\varphi_0} \frac{1}{mn\pi^2} \left\{ \cos\left(\frac{m\pi a_2(i)}{a}\right) - \cos\left(\frac{m\pi a_1(i)}{a}\right) \right\} \left\{ \sin\left(\frac{n\pi b_2(i)}{b}\right) - \sin\left(\frac{n\pi b_1(i)}{b}\right) \right\} \text{ for } n \neq 0 \quad (50)$$

$$C'_{m0}(i) = -\frac{1}{2} \frac{\varphi(i)}{\varphi_0} \frac{1}{m\pi} \left\{ \cos\left(\frac{m\pi a_2(i)}{a}\right) - \cos\left(\frac{m\pi a_1(i)}{a}\right) \right\} \frac{[b_2(i) - b_1(i)]}{b} \quad (51)$$

$$D'_{mn}(i) = -\frac{\varphi(i)}{\varphi_0} \frac{1}{mn\pi^2} \left\{ \sin\left(\frac{m\pi a_2(i)}{a}\right) - \sin\left(\frac{m\pi a_1(i)}{a}\right) \right\} \left\{ \cos\left(\frac{n\pi b_2(i)}{b}\right) - \cos\left(\frac{n\pi b_1(i)}{b}\right) \right\} \text{ for } m \neq 0 \quad (52)$$

$$D'_{0n}(i) = -\frac{1}{2} \frac{\varphi(i)}{\varphi_0} \frac{1}{n\pi} \left\{ \cos\left(\frac{n\pi b_2(i)}{b}\right) - \cos\left(\frac{n\pi b_1(i)}{b}\right) \right\} \frac{[a_2(i) - a_1(i)]}{a} \quad (53)$$

$$D_{mn}(i) = \frac{\varphi(i)}{\varphi_0} \frac{1}{mn\pi^2} \left\{ \sin\left(\frac{m\pi a_2(i)}{a}\right) - \sin\left(\frac{m\pi a_1(i)}{a}\right) \right\} \left\{ \sin\left(\frac{n\pi b_2(i)}{b}\right) - \sin\left(\frac{n\pi b_1(i)}{b}\right) \right\} \text{ for } n \neq 0 \text{ and for } m \neq 0 \quad (54)$$

$$D_{m0}(i) = \frac{1}{2} \frac{\varphi(i)}{\varphi_0} \frac{1}{m\pi} \left\{ \sin\left(\frac{m\pi a_2(i)}{a}\right) - \sin\left(\frac{m\pi a_1(i)}{a}\right) \right\} \frac{[b_2(i) - b_1(i)]}{b} \quad (55)$$

$$D_{0n}(i) = \frac{1}{2} \frac{\varphi(i)}{\varphi_0} \frac{1}{n\pi} \left\{ \sin\left(\frac{n\pi b_2(i)}{b}\right) - \sin\left(\frac{n\pi b_1(i)}{b}\right) \right\} \frac{[a_2(i) - a_1(i)]}{a} \quad (56)$$

$$D_{00}(i) = \frac{1}{4} \frac{\varphi(i)}{\varphi_0} \frac{[a_2(i) - a_1(i)]}{a} \frac{[b_2(i) - b_1(i)]}{b} \quad (57)$$

Since the amount of energy dissipated by the heat sources is equal to the amount of energy transferred to the heat sinks, the sum of coefficient D_{00} for the heat sinks and the heat sources is equal to zero.

Appendix 2: Simplification of the temperature field depending on the configuration

Conf.	
A	<p>Central symmetry: $T^*(X, Y, Z) = T^*(-X, -Y, Z)$</p> <p>Simplifications:</p> $\sum_{i=1}^{n_{source}+n_{sink}} C_{mn}(i) = 2 \sum_{i=1}^{\tilde{n}_{source}+\tilde{n}_{sink}} C_{mn}(i)$ $\sum_{i=1}^{n_{source}+n_{sink}} C'_{mn}(i) = 0 \Rightarrow A'_{mn}(Z) = 0$ $\sum_{i=1}^{n_{source}+n_{sink}} D_{mn}(i) = 2 \sum_{i=1}^{\tilde{n}_{source}+\tilde{n}_{sink}} D_{mn}(i)$ $\sum_{i=1}^{n_{source}+n_{sink}} D'_{mn}(i) = 0 \Rightarrow B'_{mn}(Z) = 0$ <p>Temperature field expression:</p> $T^*(X, Y, Z) = \sum_{m=1}^{\infty} \sum_{n=1}^{\infty} A_{mn}(Z) \sin(m\pi X) \sin(n\pi Y) + \sum_{m=0}^{\infty} \sum_{n=0}^{\infty} B_{mn}(Z) \cos(m\pi X) \cos(n\pi Y)$
B	<p>Two axial symmetries: $T^*(X, Y, Z) = T^*(-X, Y, Z)$ $T^*(X, Y, Z) = T^*(X, -Y, Z)$</p> <p>Simplifications:</p> $\sum_{i=1}^{n_{source}+n_{sink}} C_{mn}(i) = 0 \Rightarrow A_{mn}(Z) = 0$ $\sum_{i=1}^{n_{source}+n_{sink}} C'_{mn}(i) = 0 \Rightarrow A'_{mn}(Z) = 0$ $\sum_{i=1}^{n_{source}+n_{sink}} D_{mn}(i) = 4 \sum_{i=1}^{\tilde{n}_{source}+\tilde{n}_{sink}} D_{mn}(i)$ $\sum_{i=1}^{n_{source}+n_{sink}} D'_{mn}(i) = 0 \Rightarrow B'_{mn}(Z) = 0$ <p>Temperature field expression:</p> $T^*(X, Y, Z) = \sum_{m=0}^{\infty} \sum_{n=0}^{\infty} B_{mn}(Z) \cos(m\pi X) \cos(n\pi Y)$
C	<p>One axial symmetry: $T^*(X, Y, Z) = T^*(-X, Y, Z)$</p> <p>Simplifications:</p> $\sum_{i=1}^{n_{source}+n_{sink}} C_{mn}(i) = 0 \Rightarrow A_{mn}(Z) = 0$ $\sum_{i=1}^{n_{source}+n_{sink}} C'_{mn}(i) = 0 \Rightarrow A'_{mn}(Z) = 0$ $\sum_{i=1}^{n_{source}+n_{sink}} D_{mn}(i) = 2 \sum_{i=1}^{\tilde{n}_{source}+\tilde{n}_{sink}} D_{mn}(i)$ $\sum_{i=1}^{n_{source}+n_{sink}} D'_{mn}(i) = 2 \sum_{i=1}^{\tilde{n}_{source}+\tilde{n}_{sink}} D'_{mn}(i)$ <p>Temperature field expression:</p> $T^*(X, Y, Z) = \sum_{m=0}^{\infty} \sum_{n=1}^{\infty} B'_{mn}(Z) \cos(m\pi X) \sin(n\pi Y) + \sum_{m=0}^{\infty} \sum_{n=0}^{\infty} B_{mn}(Z) \cos(m\pi X) \cos(n\pi Y)$